Journal of Alloys and Compounds 509 (2011) 6021–6029

Contents lists available at ScienceDirect

Journal of Alloys and Compounds

journal homepage: www.elsevier.com/locate/jallcom

Microstructure and mechanical properties of magnesium composites prepared by spark plasma sintering technology

Wan Nur Azrina Wan Muhammad [a,b], Zainuddin Sajuri [c,*], Yoshiharu Mutoh [d], Yukio Miyashita [d]

[a] Department of Mechanical Engineering, Nagaoka University of Technology, 1603-1 Kamitomioka, Nagaoka-shi 940-2188, Japan
[b] Department of Materials Engineering & Design, Faculty of Mechanical Engineering and Manufacturing, Universiti Tun Hussein Onn Malaysia, 86400 Batu Pahat, Johor, Malaysia
[c] Department of Mechanics and Materials Engineering, Faculty of Engineering and Built Environment, Universiti Kebangsaan Malaysia, 43600 Bangi, Selangor, Malaysia
[d] Department of System Safety, Nagaoka University of Technology,1603-1 Kamitomioka, Nagaoka-shi 940-2188, Japan

ARTICLE INFO

Article history:
Received 20 August 2010
Received in revised form 24 February 2011
Accepted 25 February 2011
Available online 5 March 2011

Keywords:
Composite material
Magnesium
AZ31 alloy
SiC particle
Powder metallurgy
Spark plasma sintering
Mechanical properties

ABSTRACT

Spark plasma sintering (SPS) technology was used to determine the appropriate conditions for SPS sintering of commercially pure magnesium as well as the magnesium alloy AZ31. It was found that the sintering temperatures of 585 °C and 552 °C were the most suitable sintering temperatures for the magnesium and the AZ31 alloy, respectively. Magnesium matrix and AZ31 alloy matrix composites reinforced with SiC particles were then successfully fabricated by the SPS method at sintering temperatures of 585 °C and 552 °C, respectively. A uniform distribution of SiC particles was observed along the boundary between matrix particles. The mechanical properties, i.e. hardness and tensile strength increased with increasing SiC content up to 10 wt%. However, when the SiC content was larger than 10 wt%, the tensile strength decreased due to the agglomeration of SiC particles. The agglomeration of SiC particles was found to lead to the degradation of the interfacial bonding strength between matrix and reinforcement.

1. Introduction

Magnesium and its alloys are of interest because of their low density, 1.74 g/cm^3, and high specific strength as compared to other structural metals. These properties are important in automotive and aerospace applications in order to reduce fuel consumption and to reduce green house emission [1]. Magnesium and its alloys also possess several other benefits including tensile strength values comparable to those of with aluminum alloys, high damping capacity, machinability, a low production energy requirement in comparison with aluminum [2]. The main limitations of magnesium and its alloys are their low ductility and rapid loss of strength at high temperatures which limits their use in conventional and critical engineering applications as a structural material.

Enhancement in mechanical properties of magnesium could be obtained by incorporation of temperature-stable reinforcements in the magnesium matrix. Since magnesium composites have several advantages compared to monolithic magnesium and its alloys, numerous studies have been conducted on magnesium based composites [3–11]. Hassan et al. [10] studied microstructure and mechanical properties of the magnesium reinforced with Y_2O_3. Habibnejad et al. [1] investigated mechanical properties of the magnesium composites reinforced with Al_2O_3 nanoparticles. Paramsothy et al. [12] synthesized the AZ31 composites reinforced with Al_2O_3 to obtain improved mechanical properties of composites. Deng et al. [13] improved microstructure and mechanical properties of AZ91 composites through the addition of submicron size silicon carbide particles. Silicon carbide (SiC) is particularly attractive as a reinforcing phase due to high hardness which improves the room and elevated temperature mechanical properties as well as wear resistance [14].

Magnesium based composites have been produced by variety of methods; stir casting, disintegrated metal deposition, melt infiltration, powder metallurgy, etc. Many previous research programs have shown that powder metallurgy technique is an important and useful processing route for fabrication of composites. Powder metallurgy is an advanced metal forming technology used for producing high quality structural components with near net shape [15], and a number of researchers have used the powder metallurgy technique for fabricating magnesium based composites. Wong and Gupta [2] synthesized magnesium composites with copper particulates by using a powder metallurgy technique which involved microwave assisted two-directional sintering. Fukuda et al. [16] fabricated magnesium alloy AZ61 composites which were reinforced with carbon nanotube using powder metallurgy based upon wet processing. Powder metallurgy can become an even better fab-

* Corresponding author. Tel.: +81 0258 47 9003; fax: +81 0258 47 9010.
E-mail address: mutoh@mech.nagaokaut.ac.jp (Z. Sajuri).

0925-8388/$ – see front matter © 2011 Elsevier B.V. All rights reserved.
doi:10.1016/j.jallcom.2011.02.153

rication method if sintering were faster, cleaner and less prone to porosity and defects [17]. Spark plasma sintering (SPS) is a promising technique that is aimed at fulfilling the above mentioned conditions.

Spark plasma sintering (SPS), also known as a pulse electric current sintering, is an advanced process which can significantly improve the quality of sintered samples. The main advantages of SPS are that a high temperature is generated locally, the heating rate is rapid. In SPS process, pulse electrical current flows directly in the sintered materials and graphite mold and generate plasma in a gap or at the contact point between particles. A very high heating efficiency is offered and a high quality sintered specimen is easily obtained at a lower sintering temperature and in a shorter time than the conventional process [18]. Zadra et al. [19] fabricated aluminium bulk materials by spark plasma sintering and found that mechanical properties and fracture morphology of the sintered aluminium prepared by SPS process were very similar to those of pure annealed wrought aluminium. Kondoh et al. [20] fabricated pure titanium matrix composites reinforced with multi wall carbon nanotubes by SPS method. The composite materials showed an extremely high tensile strength and a good elongation at room temperature. Song et al. [21] also fabricated magnesium based composites by SPS and revealed that SPS played important role in the improvement of hydrogen storage properties of these magnesium based composites. However, no research work on microstructure and mechanical properties of magnesium and its alloy based composites reinforced with silicon carbide fabricated by using SPS technology has been reported.

In a previous paper [22], the applicability and effectiveness of SPS for fabricating magnesium and its alloys have been confirmed. Magnesium and its alloys when sintered by an SPS method exhibited a fine microstructure and excellent mechanical properties compared to those sintered by a conventional pressureless sintering method. In the present study, the magnesium and AZ31 magnesium alloy matrix composites reinforced with SiC particles were fabricated by an SPS method, and the effects of sintering temperature and SiC content on microstructure and mechanical properties were evaluated.

2. Experimental procedures

2.1. Materials and sintering process

Relatively coarse pure magnesium (Mg) powders with average particle size of 180 μm and magnesium alloy AZ31 powders with particle size ranging from 10 to 200 μm were used as matrix materials. Silicon carbide (SiC) particles with particle size ranging from 0.5 to 25 μm were used as a reinforcement phase. The weight fraction of SiC particles was in the range of 5–15 wt%. The chemical compositions of these powders are shown in Tables 1 and 2.

Prior to fabrication of the composites, suitable sintering temperatures for Mg and AZ31 alloy were determined. At first, the Mg powder was poured into a 30 mm diameter graphite die and then pre-pressed with a pressure of 10 MPa. After pre-pressing, the die was put into the chamber of SPS machine and then sintered at temperatures ranged from 455 °C to 585 °C with a pressure of 60 MPa. The heating rate was 25 °C/min and the holding time of 5 min. At sintering temperatures lower than 525 °C for Mg and 455 °C for AZ31 alloy, the porosity was high. On the other hand, when the sintering temperatures were higher than 585 °C and 552 °C for Mg and AZ31 alloy, respectively, porosity was greatly reduced during the SPS process. Accordingly, the adopted sintering temperature ranges were from 525 °C to 585 °C and from 455 °C to 552 °C for Mg and AZ31 alloy, respectively. The maximum sintering temperatures of 585 °C and 552 °C were lower than the melting temperature of magnesium (650 °C). However, the local temperature in the contact area of particles would be higher as compared as to the overall nominal temperature since the sintering temperature was measured using thermocouple not inside the die but on the graphite die surface.

In case of the composites, the Mg powders and the SiC particulates were mixed by using a rotating ball milling machine under a rotating speed of 84 rpm for 6 h without using any balls or process agents to avoid heat generation during mixing. The mixed powders were then subjected to the same sintering process described above. The same sintering process was also adopted for AZ31 alloy composite. In the present study, a Mg composite with SiC particles and the AZ31 alloy composite with SiC particles are denoted as Mg–SiC composite and AZ31–SiC composite, respectively. The final product was disc-shaped, 30 mm in diameter and 7 mm thick.

2.2. Characterization

The bulk density of the sintered sample was determined by Archimedes's principle using an electronic balancer with accuracy of ±0.0001 g. Optical microscopy was used to determine for grain morphology, and scanning electron microscopy (SEM) was used to observe the distribution of SiC particles in the sintered composite samples. Prior to observation, the surface of the sample was ground with emery papers up to 1500 grit and then polished with diamond paste up to 0.25 μm. An acetic glycol solution was used as an etching solution to reveal grain boundaries of the sintered samples.

2.3. Mechanical tests

The hardness and tensile strengths of sintered samples were determined to obtain an assessment of their mechanical properties. The hardness of the specimen was determined by using a Vickers Hardness Tester with an indenting load of 0.4903 N and a holding time of 20 s. Tensile test specimens with gauge part width of 2 mm, thickness of 3 mm and length of 3 mm were machined from the disc-shape sintered samples by using an EDM machine. The tensile test was performed at crosshead speed of 0.5 mm/min. Subsequently, fracture surfaces were observed by using an SEM.

3. Results and discussion

3.1. Monolithic Mg and AZ31 alloy

3.1.1. Microstructure

Microstructures of Mg sintered at temperatures ranged from 525 to 585 °C are shown in Fig. 1. As seen from the figure, the sintered samples were well sintered without pores, while the initial particle boundaries could be observed. This suggested that the oxides still existed along the particle boundaries as they initially existed on the powder surface. However, these particle boundary oxides were tended to disappear with increasing sintering temperature. As reported by Xu et al. [23], the particle boundaries of SPS sintered aluminum alloy became less because of rupture of oxide film during spark plasma sintering process due to high pressure and high temperature in the contacting areas between particles.

Microstructures of AZ31 alloy sintered at temperatures ranged from 455 °C to 552 °C are shown in Fig. 2. The sintered samples were well sintered and no pores were detected. The particle boundary oxides could be also observed and tended to disappear with increasing sintering temperature. From the figure, it was found that grain boundaries could be clearly observed compared to the sintered Mg samples and that the grain size tended to increase with increasing sintering temperature. The difference of grain boundary appearance between Mg and AZ31 alloy will be due to the difference of chemical composition of grain boundary.

3.1.2. Relative density

Relationship between relative density and sintering temperature for Mg and AZ31 alloy sintered by the SPS method is shown in Fig. 3. It could be seen from the figure that relative density was almost constant regardless of sintering temperature. Almost full density was attained at sintering temperatures higher than 525 °C for Mg and nearly full density over 98% was attained at whole sintering temperatures for AZ31 alloy. From these results, it can be concluded that SPS is an effective technique for densification of magnesium and its alloys.

3.1.3. Hardness

Relationship between Vickers hardness and sintering temperature for Mg and AZ31 alloy sintered by the SPS method is shown in Fig. 4. The values of Vickers hardness for both the sintered Mg and AZ31 alloy were almost constant regardless of sintering temperature. Hardness of sintered materials may depend on volume fraction of porosity (relative density) and grain size. As shown in

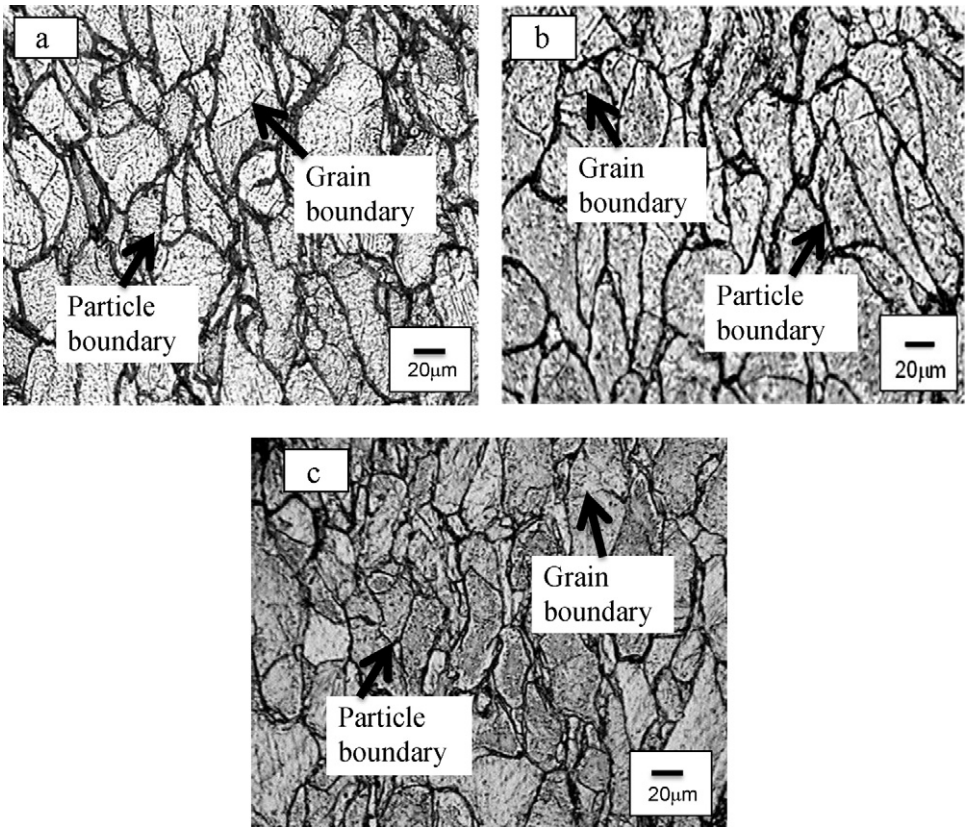

Fig. 1. Microstructures of the Mg samples sintered at 525 °C, 552 °C and 585 °C by SPS.

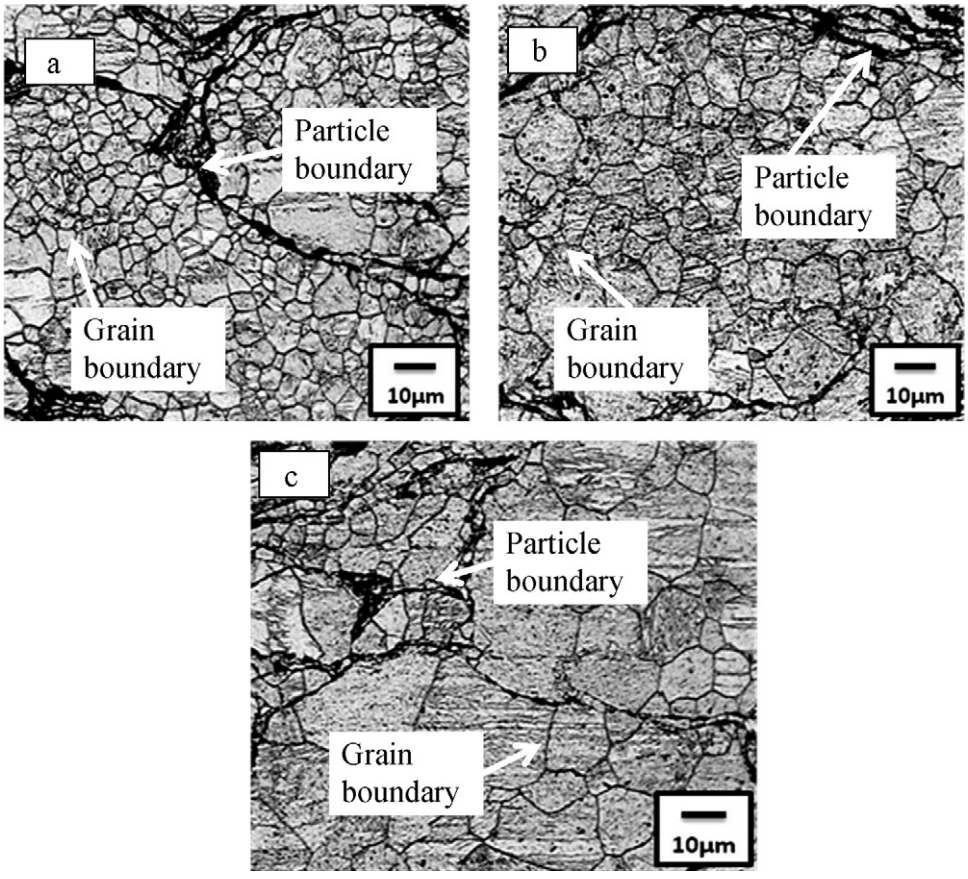

Fig. 2. Microstructures of the AZ31 alloy samples sintered at (a) 455 °C, (b) 525 °C and (c) 552 °C by SPS.

Table 1
Chemical composition of the Mg and AZ31 powders.

Material	Mg (%)	Al (%)	Ca (%)	Cu (%)	Fe (%)	Mn (%)	Si (%)	Zn (%)	Other (%)
Mg	99.9	0.005	0.001	0.001	0.003	0.01	0.02	0.003	0.043
AZ31	95.4	2.96	–	0.0019	–	0.35	0.0127	0.98	0.3016

Table 2
Chemical composition of the silicon carbide powder.

Material	SiC (%)	C (%)	SiO_2 (%)	Fe (%)	Al (%)
SiC	97.3	0.05	1.32	1.15	0.005

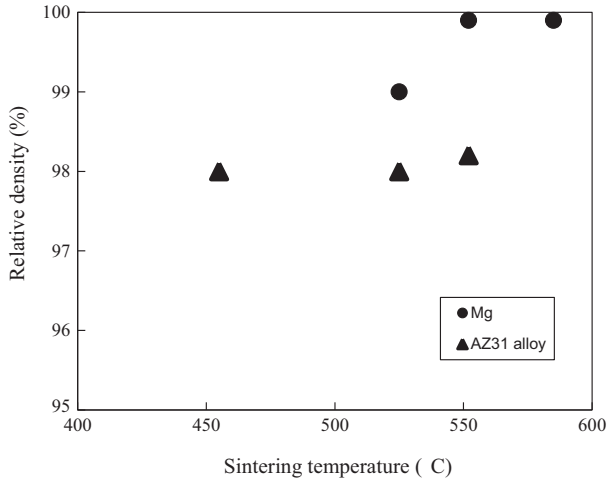

Fig. 3. Relationship between relative density and sintering temperature for the Mg and AZ31 alloy sintered by SPS.

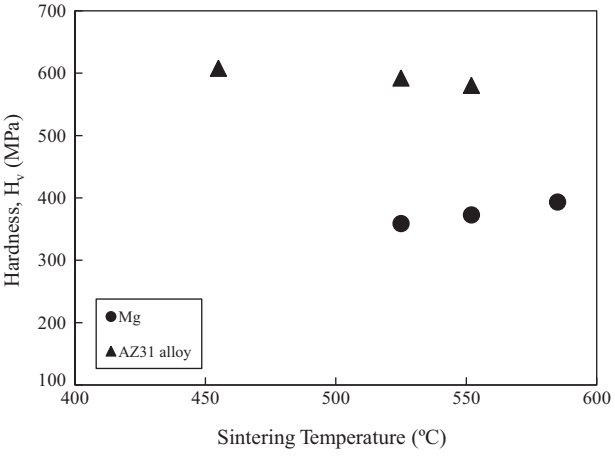

Fig. 4. Relationship between hardness and sintering temperature for the Mg and AZ31 alloy sintered by SPS.

Fig. 3, the relative density was almost constant regardless of sintering temperature. Variation of grain size with sintering temperature was not significant and within the factor of two, while it increased with increasing sintering temperature, as seen from Figs. 1 and 2. Consequently, the hardness was almost constant regardless of sintering temperature for both the Mg and AZ31 alloy samples.

3.1.4. Tensile strength

Relationship between tensile strength and sintering temperature for the Mg and AZ31 alloy sintered by SPS is shown in Fig. 5. Tensile strength was significantly improved with increasing sintering temperature for both the Mg and AZ31 alloy samples. The

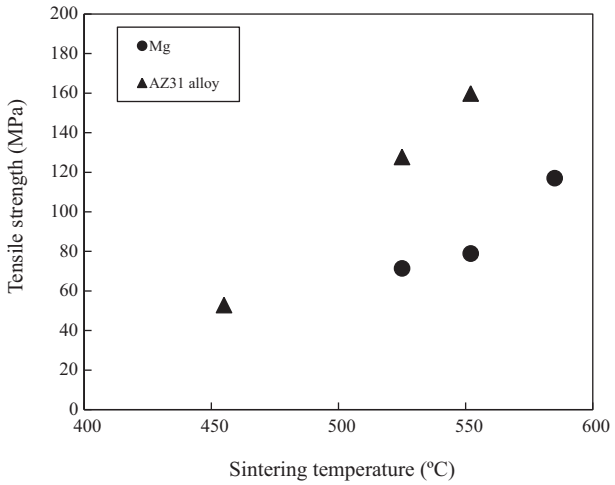

Fig. 5. Relationship between tensile strength and sintering temperature for the Mg and AZ31 alloy sintered by SPS.

highest tensile strength of 120 MPa for sintered Mg samples was obtained at a sintering temperature of 585 °C, while that of 160 MPa for the sintered AZ31 alloy samples was obtained at a sintering temperature of 552 °C. The reason why the highest tensile strength for Mg sample was obtained at 585 °C, which was higher than the temperature achieving full density (552 °C), would be as follows: even after achieving full density, tensile strength would depend on the nature of powder boundary. Much strong bonding between powders would be achieved with increasing sintering temperature, where breakdown of oxide film along the powder boundary would become easier and then fraction of metal-to-metal bonding interface would be increased.

Fractographs of the Mg samples sintered by SPS at different sintering temperatures are shown in Fig. 6. As seen from the figure, fracture facets corresponding to the Mg powders were found at lower temperature (525 °C), while overall feature of fracture surface was ductile fracture. The facets were disappeared when sintering temperature became high up to 585 °C and the fracture surface looked ductile fracture which was found in bulk materials.

Fractographs of the AZ31 alloy sintered by SPS at different sintering temperatures are shown in Fig. 7. As seen from the figure, some fracture facets corresponding to the AZ31 powders were observed when the sintering temperature was low (455 °C). When the sintering temperature became high, ductile fracture surface without the powder-like facets was observed, as seen in Fig. 7c.

From the fracture surface observations, it was speculated that when the sintering temperature was low, some powder boundaries were weak due to oxide film remained on the powder surface and then influenced fracture behavior, while the oxide film and powder boundary almost disappeared and did not influence fracture behavior when the sintering temperature became high.

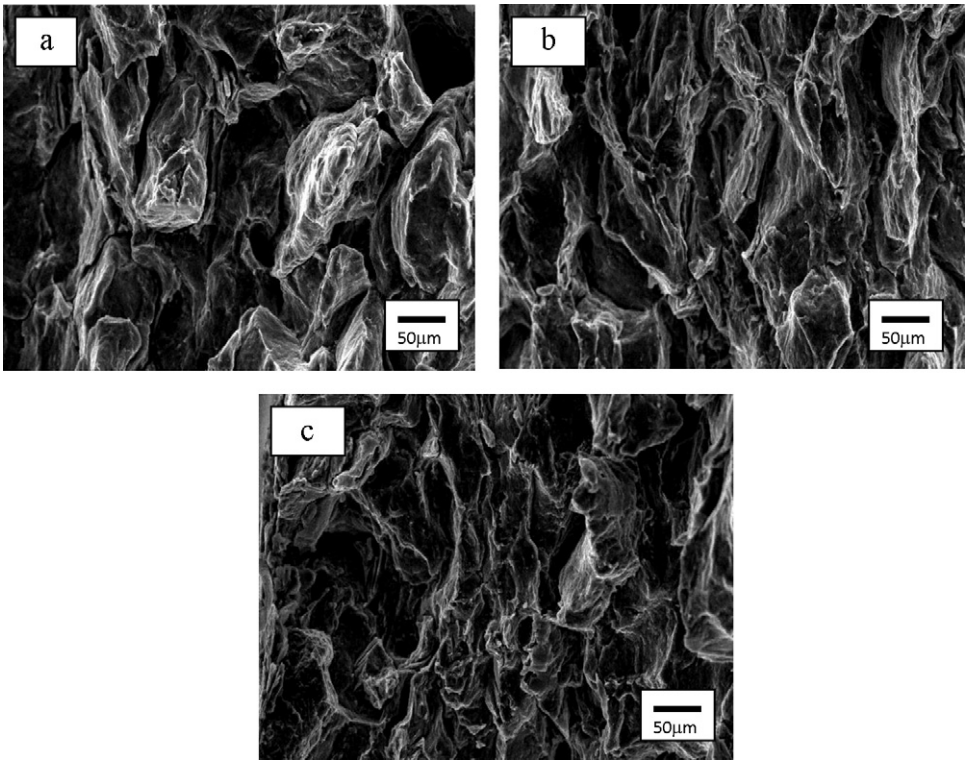

Fig. 6. Fracture surface morphology of the Mg samples sintered by SPS at different sintering temperatures: (a) 525 °C, (b) 552 °C and (c) 585 °C.

It is generally known that tensile strength is in proportion to hardness for structural materials. The hardness of the present sintered materials was almost constant regardless of sintering temperature, while the tensile strength increased with increasing sintering temperature, as seen from Figs. 4 and 5. This may result from that the oxide film on powder surface significantly influences fracture behavior, while it does not much influence plastic deformation due to indentation. Approximate relationship between tensile

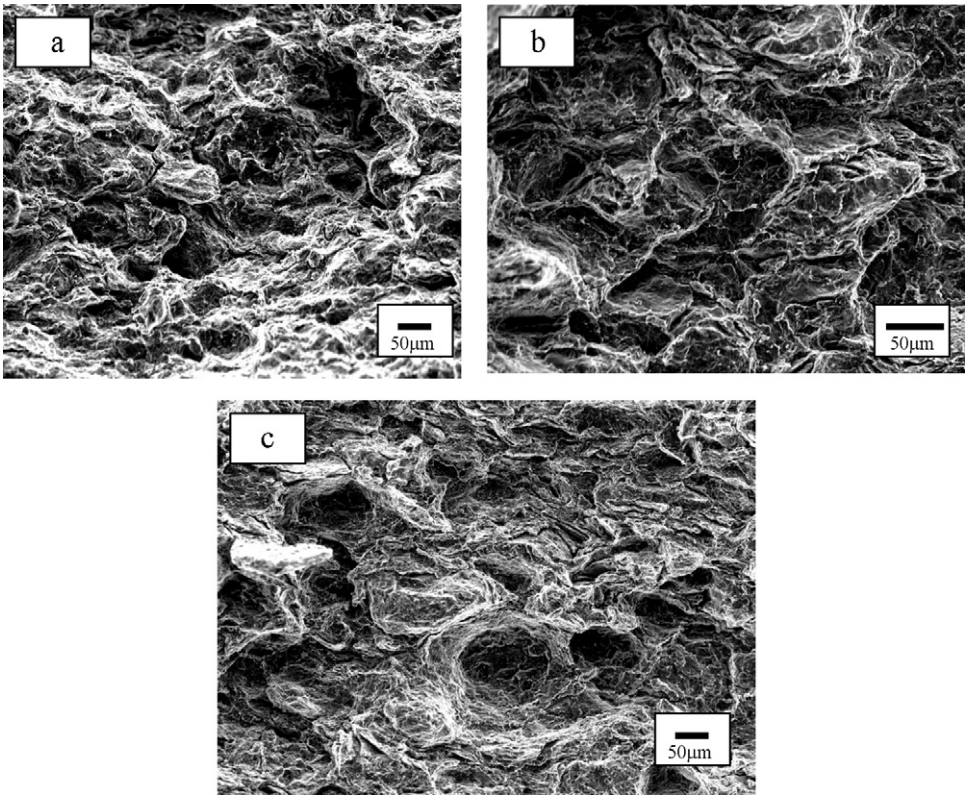

Fig. 7. Fracture surface morphology of the AZ31 alloy samples sintered by SPS at different sintering temperatures: (a) 455 °C, (b) 525 °C and (c) 552 °C.

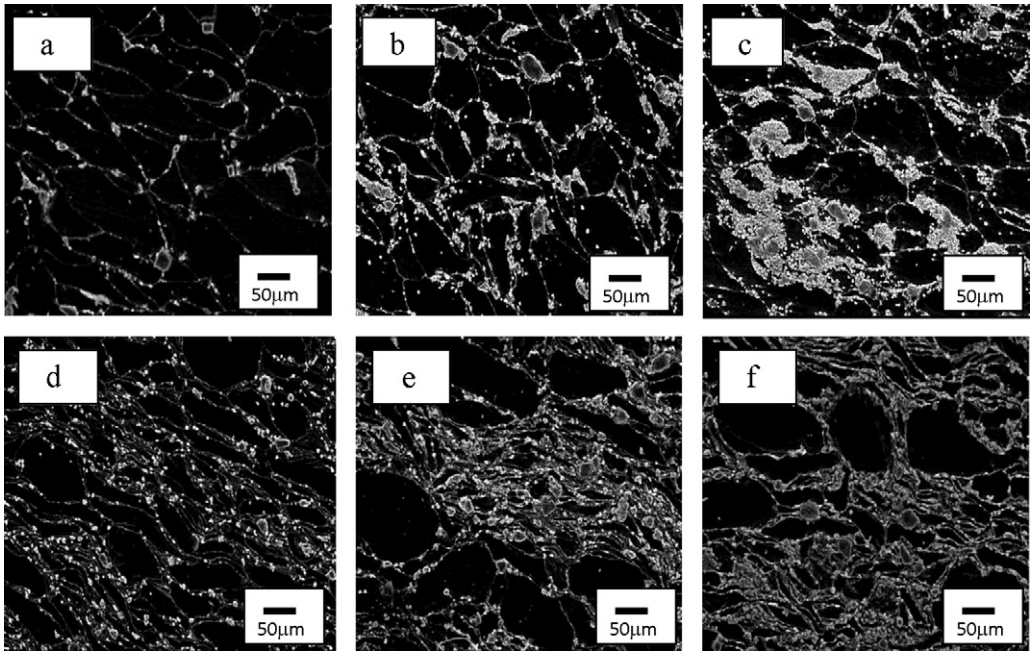

Fig. 8. SEM micrographs of the Mg-SiC composites with (a) 5 wt%SiC, (b) 10 wt%SiC, (c) 15 wt%SiC and the AZ31-SiC composites with (d) 5 wt%SiC, (e) 10 wt%SiC, (f) 15 wt%SiC. Loading direction of SPS is vertical.

strength and hardness for structural materials has been proposed as: $\sigma_B = HV/3$ [24]. The present sintered materials almost satisfied this relationship at high sintering temperature, while the tensile strength of the sample sintered at lower sintering temperature was rather low compared to that estimated from one third of hardness. Therefore, the present Mg and AZ31 alloy sintered at 585 °C and 552 °C, respectively, were considered to be high quality materials with full density and no influence of oxide film.

3.2. Mg–SiC and AZ31–SiC composites

From the foregoing results and discussion, the appropriate sintering temperatures for Mg and AZ31 alloy were determined as 585 °C and 552 °C, respectively. Based on this result, Mg–SiC and AZ31–SiC composites were sintered at 585 °C and 552 °C, respectively, by using SPS process. Observation of microstructure, density measurement, hardness test and tensile test of the sintered composites were carried out.

3.2.1. Microstructure

Examples of SEM microstructure observations of the Mg–SiC composites and the AZ31–SiC composites sintered at 585 °C and 552 °C, respectively, are shown in Fig. 8. As seen from the figure, SiC particles were almost uniformly distributed along the boundary of the magnesium and AZ31 alloy powders when the SiC content was less than 10 wt%. An SEM micrograph of SiC–Mg interface for the Mg–SiC composite with 10 wt% of SiC content is shown in Fig. 9. No void and only intimate contact were observed at interface between Mg and SiC particles. From energy dispersive spectroscopy (EDS) analysis, formation of reaction products such as MgO or $MgSi_2$ was not observed at the interface, which could degrade mechanical properties of the Mg-based composites [25]. When increasing the content of SiC particles up to 15 wt%, inhomogeneous agglomerations of SiC particles were detected for both the composites, while those in the Mg–SiC composite were more significant compared to those in the AZ31–SiC composite. The agglomerations of reinforcement particles might result from the inadequate ratio of surface area between matrix alloy powders and SiC particles [26]. Zhang et al. [27] have reported for aluminium matrix composites that agglomerations of SiC particles were not electrically conductive during SPS process and then inhibited the generation of spark plasma phenomenon between SiC and matrix aluminum, which would result in the weak interfacial bonding between matrix and reinforcement.

3.2.2. Relative density

Relationship between relative density and content of SiC particle for the Mg–SiC and the AZ31–SiC composites is shown in Fig. 10. As seen from the figure, the Mg–SiC composite was almost fully dense up to the SiC content of 10 wt%. However, relative density of the Mg–SiC composites reduced to 95% when the SiC content further increased up to 15 wt%. This would result from the significant agglomerations of SiC powders, as mentioned in the previous section. On the other hand, the AZ31–SiC composite was almost fully dense regardless of SiC content up to 15 wt%.

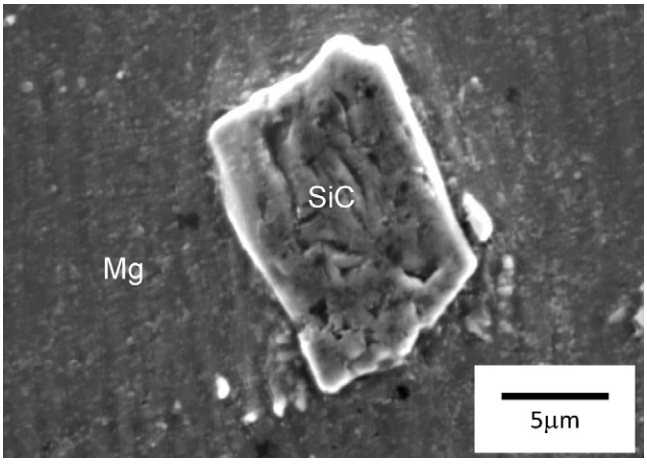

Fig. 9. An SEM micrograph of SiC–Mg interface for the Mg–SiC composite with 10 wt% of SiC content.

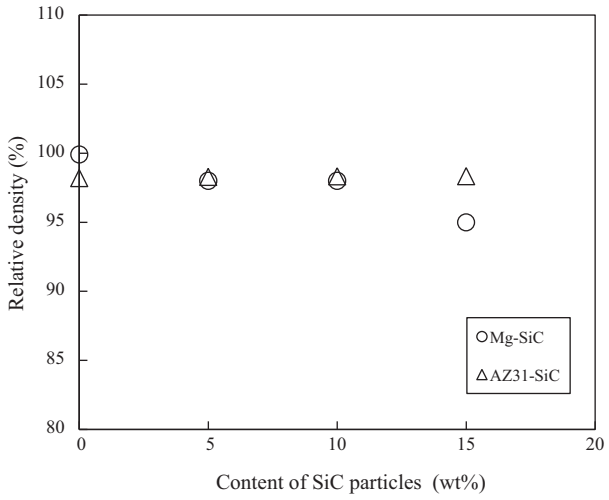

Fig. 10. Relationship between relative density and content of SiC particles.

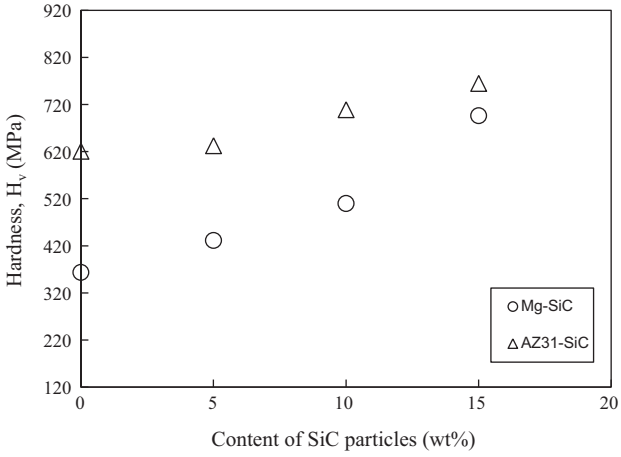

Fig. 11. Relationship between hardness and SiC content.

3.2.3. Hardness

Relationship between hardness and content of SiC particle is shown in Fig. 11. As seen from the figure, hardness significantly increased with increasing content of SiC particle for both the composites. Ugandhar et al. [28] also showed the increase in hardness with increasing SiC content for Mg–SiC composite synthesized by using a disintegrated melt deposition technique followed by hot extrusion. The hardness obtained by their experiments was about 550 MPa for the SiC content of 15 wt%. This value was lower than the hardness of 700 MPa obtained in the present study, which might also indicate the superiority of SPS process. The higher constraint of localized matrix deformation due to the increased content of SiC particle would contribute to the increase in hardness of the composite [28].

3.2.4. Tensile strength

Relationship between tensile strength and SiC content for the Mg–SiC and the AZ31–SiC composites is shown in Fig. 12. As seen from the figure, tensile strength of both the composites increased

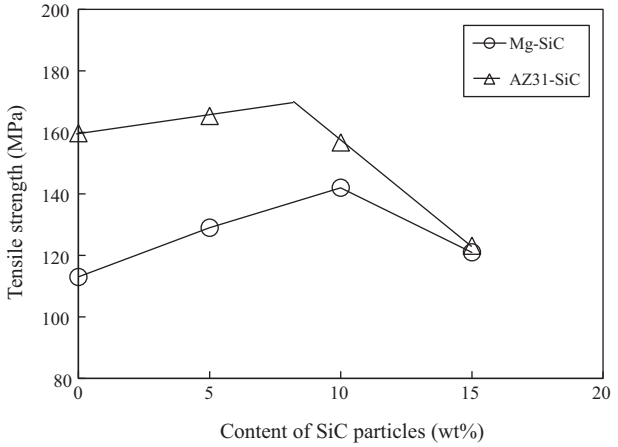

Fig. 12. Relationship between tensile strength and SiC content for the Mg–SiC and AZ31–SiC composites.

Table 3
Comparison of tensile strength of Mg-based composites.

Process	Material	Tensile strength (MPa)	Increment rate (%)	Ref.
PLS[a] + extrusion + aging	Mg	190		[6]
	Mg–10SiC (particle sized 15–38 μm)	120–135	Reduced	
DMD[b] + extrusion (13:1)	Mg	200	–	[17]
	Mg–10.3SiC	195	Reduced	
	Mg–16.0SiC	181	Reduced	
	Mg–21.3SiC	176	Reduced	
Melt stir technique + extrusion (13:1)	Mg	196	–	[4]
	Mg–30SiC[c]	258	32	
DMD[b] + extrusion (20.25:1)	Mg	207	–	[18]
	Mg–4.8SiC	219	5.8	
	Mg–10.2SiC	221	6.8	
	Mg–15.4SiC	207	0	
DMD[b] + extrusion (13:1) + aging	Mg	207	–	[15]
	Mg–4.8SiC	233	12.6	
	Mg–15.4SiC	213	2.9	
PLS[a] + extrusion (25:1)	Mg	169	–	[19]
	Mg–1.0SiC[d]	182	7.7	
	Mg–0.5SiC[d]–0.5Al_2O_3[d]	197	16.6	
	Mg–0.3SiC[d]–0.7SiC[d]	206	21.9	
Stir casting	AZ91	Similar or lower than pure Mg		[20]
	AZ91–0.5–5SiC			

[a] Pressureless sintering.
[b] Disintegrated melt deposition.
[c] Volume percentage.
[d] No-sized reinforcement.

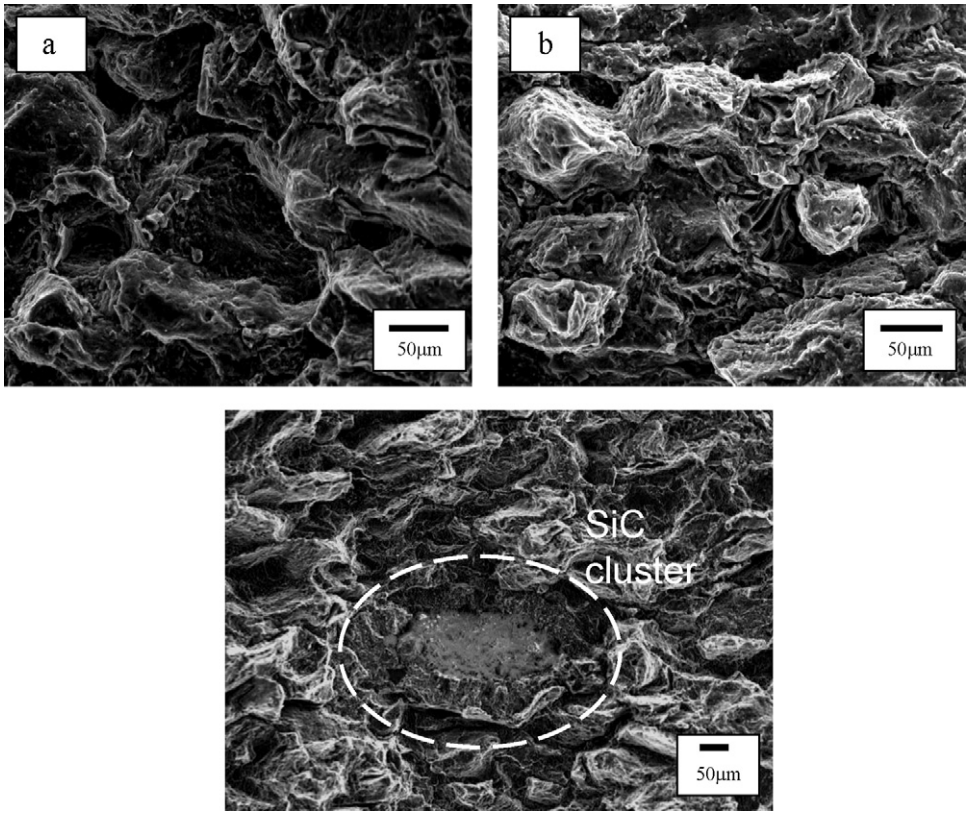

Fig. 13. Fracture surface morphology of the Mg–SiC composites with different SiC contents: (a) 5 wt%, (b) 10 wt% and (c) 15 wt%.

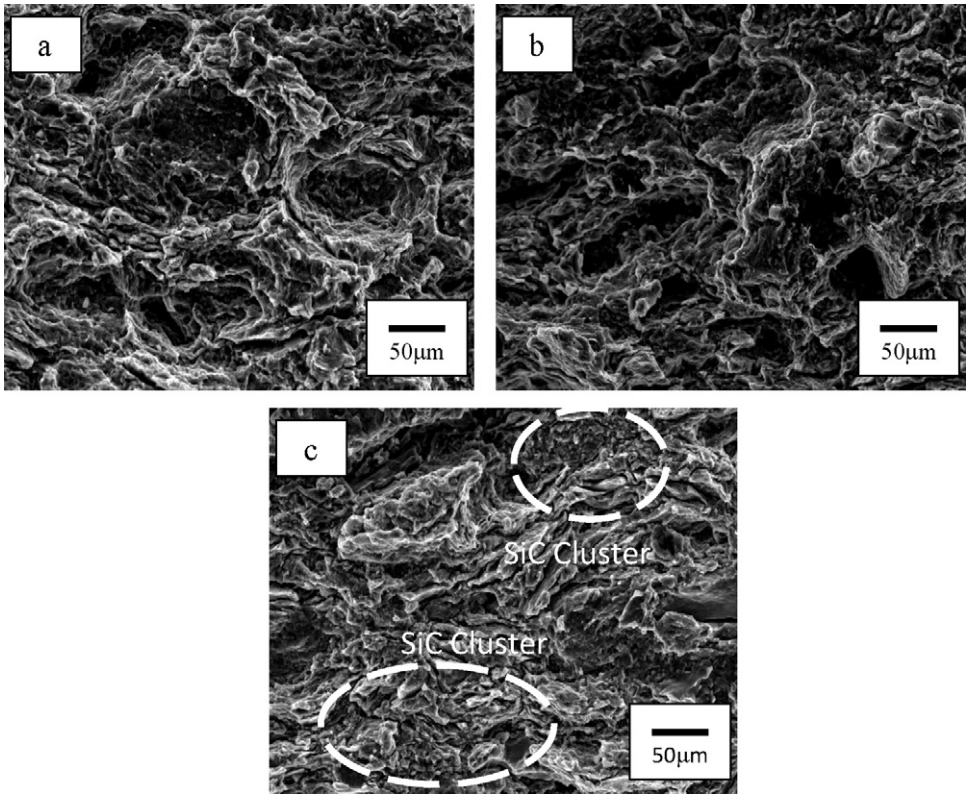

Fig. 14. Fracture surface morphology of the AZ31–SiC composites with different SiC contents: (a) 5 wt%, (b) 10 wt% and (c) 15 wt%.

with increasing SiC content. This may be due to presence of harder SiC particles, which restrict plastic deformation of the matrix. With increasing volume fraction of SiC particle, more load was transferred for plastic deformation due to constraint by SiC particles, which also resulted in a higher tensile strength of the composite [29]. When the SiC content increased to 10 wt% and about 8 wt% for the Mg–SiC and the AZ31–SiC composites, respectively, tensile strength attained the maximum value and then decreased with further increase in SiC content. The reduction of tensile strength at higher contents of SiC particle would be induced by the agglomeration of SiC particles at higher contents of SiC particles, as shown in Fig. 8.

It was found from Fig. 12 that improvement of tensile strength by addition of SiC particles was about 27% and 6.3% for the Mg-based composite and the Mg alloy based composite, respectively. Several research works on Mg-based composite with SiC particles have been reported [13,14,25,28,30–32], while their fabricating processes have been various. Table 3 shows the summary of tensile strengths of Mg-based composites reported. As seen from the table, the most successful case for improving tensile strength with addition of SiC particles and with post-process of extrusion was 32% of improvement [27] which comparable to 27% of improvement for the present Mg-based composite, which could be achieved without post-processing in the present study. The other cases showed degradation of strength or less than 20% of improvement. Therefore, SPS would be a useful process for fabricating Mg-based and Mg alloy based composites with SiC particle reinforcement.

Results of fracture surface observations for the Mg–SiC and the AZ31–SiC composites are shown in Figs. 13 and 14, respectively. As seen from the figures, fracture surface morphology looked almost similar at the SiC contents lower than 10 wt% for both the composites. However, SiC particle clusters were often found on the fracture surface when the SiC content increased to 15 wt%, as seen in Figs. 13 and 14(c). Therefore, the decrease of tensile strength would be induced by the significant agglomeration of SiC particles at higher SiC contents.

Tensile strength of both the composites initially increased and then decreased with increasing SiC content, while hardness monotonically increased with increasing SiC content. This difference of variation between tensile strength and hardness would result from that tensile strength responds to fracture resistance, while hardness responds to plastic deformation resistance, as mentioned in Section 3.1.4.

4. Conclusions

Spark plasma sintering (SPS) technique was successfully applied for fabricating magnesium (Mg) matrix and AZ31 alloy matrix composites with SiC reinforcement particles. To obtain basic information about sintering behavior of Mg and AZ31 alloy, SPS sintering of Mg and AZ31 alloy was also carried out. Main conclusions obtained are summarized as follows.

(1) Mg and AZ31 alloy were sintered by the SPS technique to find a suitable sintering temperature for SPS sintering. Almost full dense samples could be obtained in the ranges from 525 °C to 585 °C and from 455 °C to 552 °C for Mg and AZ31 alloy, respectively. Hardness values of the samples were almost constant regardless of sintering temperature in the present range of sintering temperature. On the other hand, tensile strength increased with increasing sintering temperature and the maximum values of 120 MPa for Mg and 160 MPa for AZ31 alloy were obtained at 585 °C and 552 °C, respectively. Different trend between hardness and tensile strength would result from that hardness responds to plastic deformation, while tensile strength responds to fracture resistance.

(2) Mg matrix and AZ31 alloy matrix composites reinforced with SiC particles were successfully fabricated by using the SPS technique at sintering temperatures of 585 °C and 552 °C, respectively. SiC particles were uniformly distributed along the matrix particle boundary when the SiC content was lower than 10 wt%. Agglomeration of SiC particles was often observed when the SiC content was larger than 10 wt%. Hardness of both the composites monotonically increased with increasing SiC content. Tensile strength of both the composites initially increased with increasing SiC content and then attained the maximum values (140 MPa and 170 MPa for Mg–SiC and AZ31–SiC composites, respectively) at the SiC content of around 10 wt%. When the SiC content increased further, tensile strength decreased. This decrease of tensile strength would result from agglomeration of SiC particle at higher SiC content.

Acknowledgements

The authors would like to acknowledge Sinterland Co. Ltd. for helping to use a spark plasma sintering machine. The author's are also indebted to Prof. Mc Evily, University of Connecticut, USA, for his important suggestions to improve this study.

References

[1] M. Habibnejad-Korayem, R. Mahmudi, W.J. Poole, Mater. Sci. Eng. A519 (2009) 198–203.
[2] W.L.E. Wong, M. Gupta, Comp. Sci. Technol. 67 (2007) 1541–1552.
[3] Z. Trojanova, V. Gartnerova, A. Jager, A. Namesny, M. Chalupova, P. Palcek, P. Lukac, Comp. Sci. Technol. 69 (2009) 2256–2264.
[4] M.J. Zhang, Z. Cao, X. Yang, Y. Liu, Trans. Nonferrous Met. Soc. China 20 (2010) 471–475.
[5] J. Umeda, M. Kawakami, K. Kondoh, E.-S. Ayman, H. Imai, Mater. Chem. Phys. 123 (2010) 649–657.
[6] Z. Wang, X. Wang, Y. Zhao, W. Du, Trans. Nonferrous Met. Soc. China 20 (2010) 1029–1032.
[7] M.K. Habibi, S.P. Joshi, M. Gupta, Acta Mater. 58 (2010) 6104–6114.
[8] K.S. Tun, M. Gupta, J. Alloys Compd. 487 (2009) 42–76.
[9] J. Umeda, K. Kondoh, M. Kawakami, H. Imai, Powder Technol. 189 (2009) 399–403.
[10] S.F. Hassan, K.S. Tun, M. Gupta, J. Alloys Compd. 509 (2010) 4341–4347.
[11] I. Falcon-Franco, E. Bedolla-Becerril, J. Lemus-Ruiz, J.G. Gonzalez-Rodriguz, R. Guardian, I. Rosales, Comp. B 42 (2011) 275–279.
[12] M. Paramsothy, Q.B. Nguyen, K.S. Tun, J. Chan, R. Kwok, J.V.M. Kuma, M. Gupta, J. Alloys Compd. 506 (2010) 600–606.
[13] K.K. Deng, K. Wu, Y.W. Wu, K.B. Nie, M.Y. Zheng, J. Alloys Compd. 504 (2010) 542–547.
[14] R.A. Saravanan, M.K. Surappa, Mater. Sci. Eng. A276 (2000) 108–116.
[15] A. Tanaka, S. Yoshimura, T. Fujima, K.I. Takagi, J. Phys. Conf. Ser. 176 (012045) (2009) 1–5.
[16] H. Fukuda, K. Kondoh, J. Umeda, B. Fugetsu, Comp. Sci. Technol. (2011), doi:10.1016/j.matlet.2011.03.023.
[17] S.K. Thakur, G.T. Kwee, M. Gupta, J. Mater. Sci. 42 (2007) 10040–10046.
[18] G. Xie, O. Ohashi, N. Yamaguchi, A. Wang, Metall. Mater. Trans. A 34A (2003) 2655–2661.
[19] M. Zadra, F. Casarni, F. Girardini, L. Molinari, A. Molinari, Powder Metall. 50 (1) (2007) 40–45.
[20] K. Kondoh, T. Terujirapapong, H. Imai, J. Umeda, B. Fugetsu, Comp. Sci. Technol. 69 (2009) 1077–1081.
[21] X. Song, P. Zhang, P. Pei, J. Liu, P. Li, G. Chen, Int. J. Hydro. Energy 35 (2010) 8080–8087.
[22] W.N.A.W. Muhammad, Y. Mutoh, Y. Miyashita, Adv. Mater. Res. 129–131 (2010) 266–272.
[23] C.Y. Xu, S.S. Jia, Z.Y. Cao, Mater. Charact. 54 (2005) 394–398.
[24] Y. Mutoh, K. Tanaka, Wear 125 (1988) 175–191.
[25] B.W. Chua, L. Lu, M.O. Lai, Comp. Struct. 47 (1999) 595–601.
[26] A. Slipenyuk, V.K.Yu. Milman, V. Goncharuk, J. Eckert, Acta Mater. 54 (2006) 157–166.
[27] L.M. Zhang, X.F. Gu, D.M. Zhang, M.J. Yang, Ceram. Trans. 194 (2006) 133–141.
[28] S. Ugandhar, M. Gupta, S.K. Sinha, Comp. Struct. 72 (2006) 266–272.
[29] N. Chawla, K.K. Chawla, Metal Matrix Composites, Springer Science + Business Media Inc., New York, 2006.
[30] M. Gupta, M.O. Lai, D. Saravanaranganathan, J. Mater. Sci. 35 (2000) 2155–2165.
[31] S.U. Reddy, N. Srikanth, M. Gupta, S.K. Sinha, Adv. Eng. Mater. 6 (2004) 957–964.
[32] S.K. Thakur, K. Balasubramanian, M. Gupta, J. Eng. Mater. Technol. 129 (2007) 194–199.